

Thin Layer Tissue Classification for Electronic Cleansing of CT Colonography Data

V.F. van Ravesteijn^{*,a}, F.M. Vos^{a,b}, I.W.O. Serlie^c, R. Truyen^d and L.J. van Vliet^a

^aQuantitative Imaging Group, Faculty of Applied Sciences, Delft University of Technology, Lorentzweg 1, NL-2628CJ Delft, The Netherlands, *v.f.vanravesteijn@tudelft.nl

^bDepartment of Radiology, Academic Medical Center, Amsterdam, The Netherlands

^cDepartment of Biomedical Engineering, Eindhoven University, The Netherlands

^dPhilips Healthcare, Best, The Netherlands

Abstract

CT colonography (CTC) is a rapidly evolving technique to screen for colorectal polyps. Fecal residue may occlude or, reversely, mimic polyps. Electronic cleansing aims at removing contrast-enhanced fecal residue from the image. However, thin layers of soft tissue (the colon wall or a fold) or residue are easily misclassified by current electronic cleansing methods, thereby causing holes in the colon wall or other artefacts that hamper visualization and automated detection. We present a thin layer model to detect and characterize such layers to support electronic cleansing. It is demonstrated that the model sustains robust estimation of the location and thickness of such a layer. Such thicknesses of thin layers were measured in real data sets. A lower bound on the thickness of such layers exists and was found to be 1.0 mm for our data.

1. Introduction

Adenomatous colorectal polyps are important precursors to colorectal carcinoma. Computed tomography colonography (CTC) is a rapidly evolving technique that is advocated to screen for such polyps. The preparation of patients who undergo CTC often consists of cathartic cleansing and the oral administration of a contrast agent for fecal tagging. Subsequently, the patient undergoes CT scanning prior to which the colon is distended by insufflation with room air. Several 'electronic cleansing' algorithms were introduced to automatically segment the colon surface from this data and to facilitate a 3D endoluminal view into the colon [8, 10, 11]. All these methods focused on data from patients who had undergone extensive cathartic cleansing.

Current research aims at increasing the patient's compliance by minimizing the patient preparation. However, omitting the cathartic cleansing complicates the segmentation procedure. Due to the partial volume effect, thin layers of soft tissue surrounded by residue on the one side and air on the other are hard to segment. Likewise, thin layers of contrast-enhanced fecal residue adhering to the colon surface cause a similar problem. The problem of the detection of soft tissue in the presence of fecal residue was studied before in [3], but none of the electronic cleansing algorithms have addressed the problem of thin layers explicitly. Nevertheless, thin layer characterization was studied in other CT applications [1, 4, 5, 9]. All these approaches involved a model-fitting procedure to find the thickness and position of the layer.

This paper describes a novel segmentation method that estimates these features directly from the observed data. Moreover, the potential benefit for CTC will be shown.

2. Cleansing of CTC Data

The data may be asserted to comprise three types of materials: air (A), soft tissue (T) and tagged residue (R). The mean intensities of these materials will be denoted by I_A , I_T and I_R respectively. Effectively, electronic cleansing estimates the volume fractions of these materials in each voxel [8]. Subsequently, the colon surface may be segmented by the isosurface of 50% soft tissue.

A previously proposed approach to cleansing of CTC data was based on tissue classification using the measured intensity I and the gradient magnitude I_w in the gradient direction [8]. These features form a rotation and scale-invariant feature space as shown in Fig. 1(a) (in which σ_w represents the effective scale of measure-

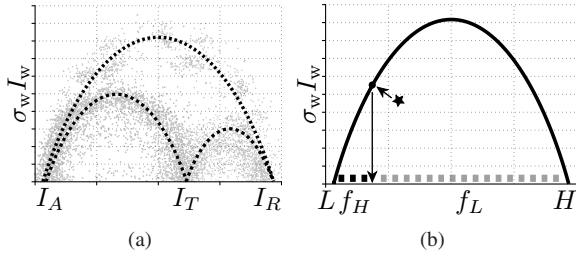


Figure 1. (a) Scatter plot of the intensity and scale-invariant gradient magnitude of voxels. The arches represent the three types of edges. (b) The material fractions are determined from the projection of a voxel onto the arch.

ment and the scale of the point spread function (PSF) in the gradient direction). Each type of edge (material transition) is represented as a different arch-shaped cloud in this feature space [2]. These arches are described by the arch-model [8]. For instance, the *A-R* transitions appear as a large arch from I_A to I_R and can be modelled by:

$$\frac{I_w}{I_R - I_A} = \frac{\sigma_w^{-1}}{\sqrt{2\pi}} \exp\left(-\text{erf}^{-1}\left(\frac{I - I_M}{I_R - I_M}\right)^2\right) \quad (1)$$

in which $I_M = (I_A + I_R)/2$.

To estimate the material constituency of a voxel, a number of voxels up and down the gradient direction are sampled. The intensity and gradient magnitude of all these voxels form a trace in $\langle I, |\nabla I| \rangle$ -space. Fitting the arch model to this measured trace yields the low L and high H material intensities, which are used to classify the transition as one of the three types. Projecting the intensity and the gradient magnitude onto the corresponding arch-model yields the material fractions f_L and f_H as indicated in Fig. 1(b).

It has been shown that this algorithm produces good results for all ‘pure’ two-material (2M) mixture transitions [8]. However, specifically a layer of soft tissue between air and residue (an *A-T-R* transition) is easily misclassified as an *A-R* transition if the layer of soft tissue is thin. We seek a model that describes such a thin layer geometry for segmentation with improved accuracy.

3. Thin Layer Model

The novelty of this paper is in the derivation of a mathematical description of a thin layer of soft tissue between air and contrast-enhanced fecal residue. Such a

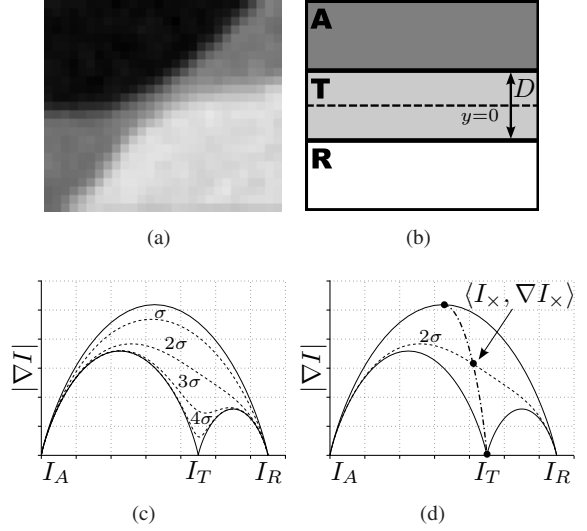


Figure 2. (a–b) A thin layer of soft tissue (gray) in CTC data and the phantom model. (c) Profiles for different thicknesses of the layer (dashed) and (d) the model for the middle of a thin layer with varying thickness (dash-dotted).

layer in real CTC data is shown in Fig. 2(a). The gradient magnitude $|\nabla I|$ and the intensity I in the phantom model (Fig. 2(b)) are computed assuming a Gaussian PSF (as done in [8]) with an effective scale $\sigma_w=1$ (notice that consequently $\sigma_w I_w$ can simply be written as $|\nabla I|$). The traces in $\langle I, |\nabla I| \rangle$ -space for different thicknesses $D=\sigma \dots 4\sigma$ of the thin layer are shown in Fig. 2(c). If the thickness $D < \sigma$ the profile resembles the profile of an *A-R* transition, whereas if the thickness $D > 4\sigma$ the profile approximates that of two separate transitions. Several features for these types of profiles will now be derived to distinguish a thin layer *A-T-R* transition from an *A-R* transition.

3.1. Description at $y = 0$

Using the assumption of a Gaussian PSF, the intensity at the middle of the layer ($y=0$) is given by

$$I(y=0; D, \sigma) = I_A \int_{-\infty}^{-D/2} g(y'; \sigma) dy' + I_T \int_{-D/2}^{D/2} g(y'; \sigma) dy' + I_R \int_{D/2}^{\infty} g(y'; \sigma) dy'$$

with $g(\cdot; \sigma)$ the Gaussian kernel. Rewriting this leads to an expression for the intensity given a thickness D :

$$\frac{I(y=0; D, \sigma) - I_M}{I_T - I_M} = \text{erf} \left(\frac{D/\sigma}{2\sqrt{2}} \right). \quad (2)$$

The gradient of the intensity at $y=0$ is given by

$$\begin{aligned} \nabla I(y=0; D, \sigma) &= g \left(\frac{D}{2}; \sigma \right) [(I_R - I_T) + (I_T - I_A)] \\ &= \frac{1}{\sigma\sqrt{2\pi}} \exp \left(-\frac{(D/2)^2}{2\sigma^2} \right) (I_R - I_A). \end{aligned} \quad (3)$$

The relation between I and ∇I at $y=0$ is obtained from eqs. 2 and 3 by eliminating D :

$$\begin{aligned} \frac{\nabla I(y=0; D, \sigma)}{I_R - I_A} &= \\ \frac{\sigma^{-1}}{\sqrt{2\pi}} \exp \left(-\text{erf}^{-1} \left(\frac{I(y=0; D, \sigma) - I_M}{I_T - I_M} \right)^2 \right). \end{aligned} \quad (4)$$

Eq. 4 has the same form as eq. 1, which describes the arches of 2M-transitions. The only difference is that the argument of the $\text{erf}^{-1}(\cdot)$ function is scaled by $(I_T - I_M)$ rather than $(I_R - I_M)$. In other words, the model delivered by eq. 4 is essentially obtained by scaling the intensity of the arch of a two-material A - R transition by $(I_T - I_M) / (I_R - I_M)$. Fig. 2(d) visualizes this relation between the gradient and intensity (dash-dotted curve). The dots along the curve indicate the feature values at $y=0$ for the thicknesses $D=0, 2\sigma$ and ∞ .

3.2. Geometric Construction

The model for the middle of the layer of soft tissue can also be obtained by adding parts of the arches of the A - T and T - R transitions. Fig. 3 illustrates this construction which consists solely of combining curves that were already presented in Figs. 2(c-d).

First, one may realize that the difference between the model of an A - R transition and the model of an A - T transition is the model of a T - R transition. This can be seen in Fig. 3(a). Starting from I_A and traversing the large arch ends in the same point as traversing the two smaller arches one after the other. Moreover, traversing from I_A to halfway an A - R transition is the same as traversing to halfway an A - T transition and subsequently traversing half of the T - R transition. This is shown geometrically by shifting half of the T - R arch onto the A - T arch (arrow 1). The same can be done for half of the A - T transition, which can be shifted onto the T - R transition (arrow 2).

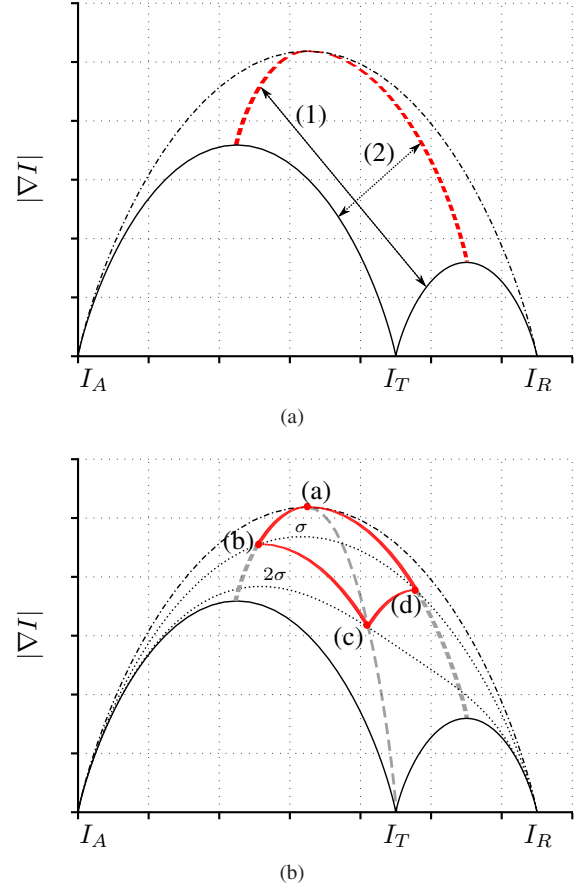


Figure 3. (a) Shifting parts of the arches describing two-material transitions. (b) Additive behavior of the arch representation. The model delivered by eq. 4 is constructed by adding parts of the T - R transition model (a - b and d - c) and the A - T transition model (b - c and a - d).

The two arches that were shifted previously touch each other halfway an A - R transition. Traversing from this point along the shifted arches is equivalent to replacing either air or residue by soft tissue starting from the middle (i.e. a layer of soft tissue is grown either extending into the air or into the residue). This is shown in Fig. 3(b). Let us start halfway the A - R transition. After replacing 1σ of residue with soft tissue (curve a - b) and subsequently replacing 1σ of air with soft tissue (curve b - c), we will end up in point c . This point is now in the middle of a 2σ A - T - R transition. This is confirmed in Fig. 3(b) as point c is on the intersection of the model of a 2σ A - T - R transition and the model describing the middle of the layer as derived in the previous section.

To conclude, the profile of the middle of the layer of

soft tissue can not only be constructed by scaling half of an A - R transition, but also by adding parts of the two other two-material transitions.

3.3. Feature Retrieval

The objective now is to derive an expression for the thickness and the location of the thin layer. This is achieved by determining the intersection of a measured profile with the curve described by eq. 4. Let us represent the crossing by $\langle I_{\times}, |\nabla I_{\times}| \rangle$ (see Fig. 2(d)). Back-projecting this point into the image renders the location where $y=0$. The thickness of the layer may be obtained by substituting I_{\times} into eq. 2. Solving for D gives

$$D = \sigma 2\sqrt{2} \left\{ \operatorname{erf}^{-1} \left(\frac{I_{\times} - I_M}{I_T - I_M} \right) \right\}. \quad (5)$$

Alternatively, D may be obtained as a function of $|\nabla I_{\times}|$ by inverting eq. 3:

$$D = \sigma 2\sqrt{2} \sqrt{\log \left(\frac{I_R - I_A}{\sigma \sqrt{2\pi} |\nabla I_{\times}|} \right)}. \quad (6)$$

The two approaches will give exactly the same solution since $\langle I_{\times}, |\nabla I_{\times}| \rangle$ lies on the curve given by eq. 4. It may be noticed that the relation between $|\nabla I|$ and I at $y=0$ will lead to the best resolution in determining D , because the maximal separation of the thickness profiles is obtained at $y=0$ (see Fig. 2).

4. Experiments

The electronic cleansing method described previously [8] was applied to four CT colonography data sets. All A - R transitions detected (as described in Section 2) were examined in more detail. While doing so, only those transitions were retained that were at least 5 voxels away from another type of edge. This was done to reject potential three-material 'junctions' [6, 7] not complying to the thin layer model. Furthermore, only objects were included consisting of more than 10 voxels.

From each object-voxel a trace was generated in the positive and negative direction of the gradient vector until the gradient magnitude was smaller than some threshold. The intensities at the lower side (L) and the upper side (H) were at the basis to scale the encountered intensities into the $[0, 1]$ range. Moreover, all traces were made invariant to the effective scale of the measurement by multiplying the sampled gradient magnitude with σ_w . Finally, a third-order polynomial was fitted to the transformed samples to represent the profile around ' $y=0$ '. The crossing point of this polynomial with the function of eq. 4 was determined, which, in turn, yielded the location and thickness of the thin layer under consideration (see Section 3).

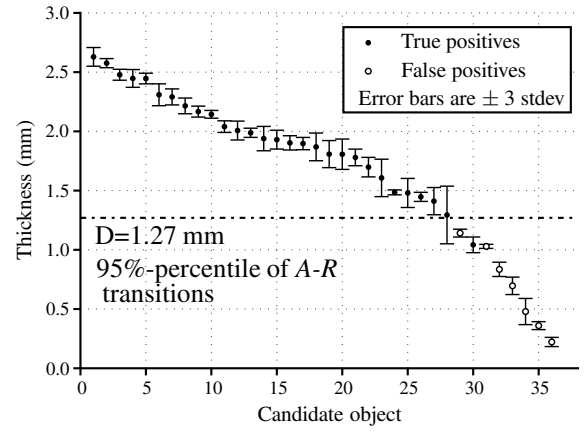


Figure 4. Mean and stdev of estimated thicknesses of the candidate objects.

5. Results

In total 411 candidate objects were generated of which 80 had a finite measured thickness. From these, 53 candidates resided in the large intestine, whereas the other 27 were associated with the small intestine. The latter fall outside the scope of CTC. 17 candidates from the 53 were found to be heterogeneously composed (by visual inspection), i.e. they comprised either a mixture of different geometries, like a fold separating air and residue and a pure 2M transition (see below for further treatment of these objects), or they consisted of an incompatible geometry like a thin layer of contrast. Thus, 36 candidate objects remained.

The mean measured thickness and corresponding standard deviation for the 36 candidate objects are shown in Fig. 4. The standard deviation emanates from averaging over the traces generated from all the object-voxels. From the same data sets, the seven largest objects consisting of traces of 'pure' A - R material transitions were analyzed. These transitions yielded a measurement of only 0.03 mm and a standard deviation ranging from 0.8–1.1 mm. The 95% percentile-level of the thickness distribution was at 1.27 mm. Accordingly, an object is considered an A - T - R transition if the mean estimated thickness of the soft tissue layer is significantly larger than 1.27 mm. Applying this procedure to the data in Fig. 4 yields a detection sensitivity of 93% (27/29), and no false positive detections. No previously discarded candidates were considered to contain a thin layer of soft tissue (by visual inspection).

The 19 objects consisting of a mixture of geometries yielded large standard deviations with respect to thickness measurement. These geometries were separated

by an EM-clustering algorithm based on the measured thickness for each profile and the spatial relation between the voxels. Fig. 5 shows the results for such an object (a fold surrounded by air and residue, both are not shown). Fig. 5(a) shows a cross-section of the object. For each voxel, represented by a dot, a trace is measured and all measurements constituting the traces are shown in Fig. 5(b). The result of clustering the traces is indicated by the color. Notice that the grouped voxels indeed form clusters in x-y space and that the traces are well separated: one cluster of traces showing normal two-material A - R transitions (gray) and another cluster showing thin layers of soft tissue with varying thickness (black). The calculated thickness was close to zero for the A - R transition and 1.8 mm for the A - T - R transition. The latter value may be negatively biased, though, due to the profiles near the transition area.

6. Conclusions

We introduced a novel method for detection and characterization of thin layers and applied it to CT colonography data. The technique may preclude erroneously removing thin layers of soft tissue (sandwiched between air and contrast-enhanced residue) and disturbing the topology of an object. A mathematical function was derived relating the intensity to the gradient magnitude in the middle of a thin layer as a function of the thickness. Practically, a layer's thickness was obtained by intersecting a measured curve in $\langle I, \sigma_w I_w \rangle$ -space with a function describing the middle of the layer. We demonstrated the usefulness of the method by first detection of thin layers of soft tissue and subsequent estimation of the thickness of these layers surrounded by residual matter and air. Observe that the method could equally well be applied to thin layers of contrast material stuck to the colon surface and surrounded by air. In future research, we will include the algorithm in an electronic cleansing algorithm for CT colonography.

References

- [1] Y. Cheng, Y. Sato, H. Tanaka, T. Nishii, N. Sugano, H. Nakamura, H. Yoshikawa, S. Wang, and S. Tamura. Accurate thickness measurement of two adjacent sheet structures in CT images. *IEICE Trans. Inf. & Syst.*, E90-D(1):271–281, 2007.
- [2] G. Kindlmann and J. W. Durkin. Semi-automatic generation of transfer functions for direct volume rendering. In *Proc. IEEE Symp. Volume Visualization*, pages 79–86, October 1998.
- [3] J. Näppi and H. Yoshida. Adaptive correction of the pseudo-enhancement of CT attenuation for fecal-

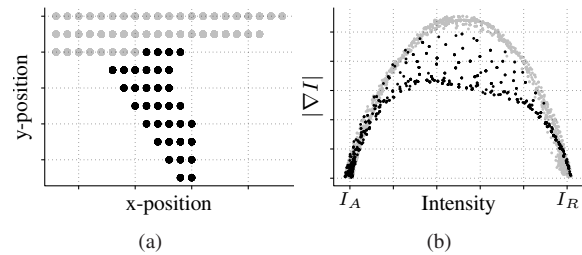


Figure 5. Heterogeneous candidate object. (a) Clustering shows two distinct regions. (b) Points on traces for both clusters.

- tagging CT colonography. *Medical Image Analysis*, 12:413–426, 2008.
- [4] S. Prevrhal, J. C. Fox, J. A. Shepherd, and H. K. Genant. Accuracy of CT-based thickness measurement of thin structures: Modeling of limited spatial resolution in all three dimensions. *Med. Phys.*, 30(1):1–8, 2003.
- [5] J. M. Reinhardt, N. D. D’Souza, and E. A. Hoffman. Accurate measurement of intrathoracic airways. *IEEE Trans. Med. Imag.*, 16(6):820–827, 1997.
- [6] I. W. O. Serlie, A. H. de Vries, F. M. Vos, Y. Nio, R. Truyen, J. Stoker, and L. J. van Vliet. Lesion conspicuity and efficiency of CT colonography with electronic cleansing based on a three-material transition model. *AJR (accepted)*, 2008.
- [7] I. W. O. Serlie, R. Truyen, J. Florie, F. H. Post, L. J. van Vliet, and F. M. Vos. Computed cleansing for virtual colonoscopy using a three-material transition model. In *Proc. MICCAI’03*, volume LNCS 2879, pages 175–183, 2003.
- [8] I. W. O. Serlie, F. M. Vos, R. Truyen, F. H. Post, and L. J. van Vliet. Classifying CT image data into material fractions by a scale and rotation invariant edge model. *IEEE Trans. Image Process.*, 16(12):2981–2994, 2007.
- [9] G. J. Streekstra, P. Brascamp, C. van der leij, R. ter Wee, S. D. Strackee, M. Maas, and H. W. Venema. Cartilage thickness measurement in the sub-millimeter range. In *Proc. MICCAI’04*, volume LNCS 3217, pages 950–958, 2004.
- [10] Z. Wang, Z. Liang, X. Li, L. Li, B. Li, D. Eremina, and H. Lu. An improved electronic colon cleansing method for detection of colonic polyps by virtual colonography. *IEEE Trans. Biomed. Eng.*, 53(8):1635–1646, 2006.
- [11] M. E. Zalis, M. A. Barish, J. R. Choi, A. H. Dachman, H. M. Fenlon, J. T. Ferrucci, S. N. Glick, A. Laghi, M. Macari, E. G. McFarland, M. M. Morrin, P. J. Pickhardt, J. Soto, and J. Yee. CT colonography reporting and data system: A consensus proposal. *Radiology*, 236:3–9, 2005.